Application of Annihilation Coincidence Detection to Transaxial Reconstruction Tomography

David W. Townsend[1] and Terry Jones[2]

[1]National University of Singapore (retired), Singapore, Singapore; and [2]University of California, Davis, California

The seminal paper by Phelps, Hoffman, Mullani, and Ter-Pogossian (*1*) from Washington University, St. Louis, appeared just a couple of years after Godfrey Hounsfield presented the first CT images using x-rays. The CT scanner was a breakthrough that demonstrated the feasibility of imaging cross-sections of the human body without interference from the sections above and below. Even before Hounsfield's pioneering CT device, David Kuhl and coworkers were exploring such a tomographic approach using single-photon counting in nuclear medicine with their Mark I–IV scintillation scanners, whereas Thomas Budinger and others used an Anger scintillation camera to acquire transaxial tomographic reconstructions. The first tomographic reconstructions using annihilation coincidence detection were obtained by David Chesler from Gordon Brownell's group at Massachusetts General Hospital using a planar positron camera designed by the Boston group. Chesler applied filtered backprojection for the first time to medical imaging in 1971.

Phelps and coworkers were the first to propose a positron emission transaxial tomograph (PETT) comprising an array of individual detectors placed around a single transaxial plane. The design acquired transaxial tomograms of the positron-emitting distribution with optimized sensitivity for that plane. Furthermore, the reconstructed images exhibited a high signal-to-noise ratio and were quantitative in that the voxel concentration of a positron emitter could actually be measured. Earlier devices suffered from high dead times and recorded elevated rates of random and scattered coincidences, thereby reducing signal-to-noise ratio. However, the St. Louis design with individual detectors achieved depth-independent spatial resolution and sensitivity, a low dead time, and a low scatter fraction by applying an energy window and axial shielding. The uptake of the positron-emitting nuclide could be quantified through attenuation correction and calibration. The

APPLICATION OF ANNIHILATION COINCIDENCE DETECTION TO TRANSAXIAL RECONSTRUCTION TOMOGRAPHY

Michael E. Phelps, Edward J. Hoffman, Nizar A. Mullani, and Michel M. Ter-Pogossian

Washington University School of Medicine, St. Louis, Missouri

465 | Number of Citations

A study was carried out to investigate the use of annihilation coincidence detection (ACD) in emission transaxial reconstruction tomography. The ACD was evaluated in terms of spatial resolution and sensitivity with depth, detection efficiency, effect of pulse-height analysis on resolution and efficiency, correction for attenuation, and cold spot contrast. A prototype positron emission transaxial tomograph (PETT) consisting of a hexagonal array of 24 NaI(Tl) detectors employing ACD was constructed. A fast Fourier transform algorithm was employed to generate the reconstructed image. Computer simulations and phantom and animal studies were carried out to demonstrate that this approach yields tomographic radionuclide images that have high resolution and contrast (hot and cold spot) and that are independent of activity above and below the plane examined. The ACD yields a quantitative nuclear medicine imaging device with high detection efficiency. Comparisons are presented between the ACD and the scintillation camera and scanner. Discussion of the possible applications of the PETT in nuclear medicine is included.

The recent introduction of the EMI scanner (*1*) has stimulated a great deal of interest in the applica-

the field of radionuclide emission imaging. Prior to the introduction of the EMI x-ray scanner, the general principle of transaxial reconstructive tomography had been applied by Kuhl and coworkers (*2–5*) to the reconstruction of radionuclide distributions in the brain. Kuhl's detection method employed a series of rectilinear scans at a number of discrete angles with collimated scintillation detectors of conventional design. This approach has since been applied with modifications by others (*6–11*). Recently, Budinger and Gullberg (*12,13*), Keyes and Simmon (*14*), and Oppenheim and Harper (*15*) presented results of transaxial tomographic reconstructions that utilized a scintillation camera.

All of the above studies of transaxial radionuclide tomography have employed single photon counting (SPC)* systems such as the scanner and scintillation camera. The work reported here deals with the application of annihilation coincidence detection (ACD)† of positron-emitting radionuclides to transaxial reconstruction tomography.

The advantages of ACD in conventional nuclear medicine imaging and transaxial reconstruction tomography have been previously reported by a number of investigators (*16–24*). Brownell and coworkers successfully developed a camera for the imaging of organs containing positron-emitting radionuclides (*18,19*). Their system has also been used to produce

substantially superior performance of the annihilation coincidence detection system was further demonstrated by comparison with single-photon counting, where depth-dependent resolution and sensitivity, a lack of attenuation correction, and low intrinsic count rates resulted in high-noise, low-resolution, nonquantitative images. This comparison highlighted the difference between the "electronic" collimation capability of annihilation coincidence detection and the need for physical collimation with single-photon counting. The feasibility and performance of the PETT design were demonstrated by imaging phantoms and a dog. The results encouraged the group to develop a larger, single-plane PETT scanner that could accommodate a human (2), demonstrating for the first time that the concentration of a positron-emitting radionuclide could be measured quantitatively and noninvasively in human tissue (3).

The impact on PETT (subsequently termed PET, positron emission tomography) of this work from St. Louis in 1975 was profound, even though at the time very few centers worldwide were exploring the use of positron-emitting nuclides for medical imaging. Nevertheless, a sustained interest in PET led Phelps and Hoffman (after they relocated from St. Louis to UCLA) to collaborate with EG&G Ortec to design and build a commercial version of their prototype (1) that became known as the ECAT II (4). Several centers worldwide invested in this device, attracted by the ability to actually measure physiologic parameters such as blood flow, oxygen utilization, glucose consumption (5), and amino acid metabolism in both health and disease. Given this paradigm shift in medical imaging, interest in PET increased, and in 1981, a refined hexagonal array for brain imaging, the NeuroECAT, was developed, again in collaboration with EG&G Ortec. Then, in 1984, the hexagonal design of the 1975 prototype was replaced with a circular array of detectors in the ECAT III PET scanner. This circular geometry would become the design standard for future PET scanners.

A major limitation of the designs described above was that each detector comprised a scintillator coupled to a photodetector, an expensive and limited solution as the demand grew for higher spatial resolution and coverage of an increased axial length of the human body by incorporating additional rings of detectors. Around 1984, Computer Technology and Imaging (CTI), a spinoff from EG&G Ortec, developed a breakthrough block detector module (6) that allowed up to 64 scintillators to be coupled to only 4 photodetectors. The block detector provided a cost-effective solution for a PET scanner design comprising multiple rings of detectors. Compared with the pioneering PETT prototype, subsequent scanner generations have incorporated better spatial resolution, greater sensitivity, faster data acquisition, lower random and scattered coincidence rates, lower detector dead time, greatly increased axial coverage, and recording of time-of-flight data. The fundamental concept of electronic collimation has been extended to fully 3-dimensional acquisition, eliminating the need for interplane shielding, and, more recently, the high-resolution molecular images have been complemented with high-resolution anatomic images through the combinations of PET/CT (in 2001) and PET/MR (in 2010).

The 24-detector PETT was able to record, within a 2.5-cm axial and approximately 16-cm transaxial field of view, only 12 coincidence lines of response at any one time, and with rotation and linear offset a total of 1,728 lines of response could be recorded for the reconstruction. At the conclusion of their paper, Phelps et al. speculated on the potential to increase the number of lines of response by extending the electronic collimation concept. Nothing illustrates the tremendous progress in PET scanner design over the past four and a half decades more than the fact that the current EXPLORER total-body PET scanner incorporates 564,480 detectors and 92×10^9 lines of response and covers 198 cm axially of the human body.

DISCLOSURE

No potential conflict of interest relevant to this article was reported.

REFERENCES

1. Phelps ME, Hoffman EJ, Mullani NA, Ter-Pogossian MM. Application of annihilation coincidence detection to transaxial reconstruction tomography. *J Nucl Med*. 1975;16:210–224.
2. Hoffman EJ, Phelps ME, Mullani NA, Higgins CS, Ter-Pogossian MM. Design and performance of a whole-body positron emission tomograph. *J Nucl Med*. 1976;17:493–502.
3. Eichling JO, Higgins CS, Ter-Pogossian MM. Determination of radionuclide concentrations with positron CT scanning (PETT): concise communication. *J Nucl Med*. 1977;18:845–847.
4. Williams CW, Crabtree MC, Burgiss SG. Design and performance characteristics of a positron emission computed axial tomograph—ECAT®-II. *IEEE Trans Nucl Sci*. 1979;26:619–627.
5. Phelps ME, Huang SC, Hoffman EJ, Selin C, Sokoloff L, Kuhl DE. Tomographic measurements of local cerebral rate in humans with (F-18) 2-fluoro-2-deoxy-D-glucose: validation of methods. *Ann Neurol*. 1979;6:371–388.
6. Casey ME, Nutt R. A multicrystal two dimensional BGO detector system for positron emission tomography. *IEEE Trans Nucl Sci*. 1986;33:460–463.

Application of Annihilation Coincidence Detection to Transaxial Reconstruction Tomography

Michael E. Phelps, Edward J. Hoffman, Nizar A. Mullani, and Michel M. Ter-Pogossian

Washington University School of Medicine, St. Louis, Missouri

A study was carried out to investigate the use of annihilation co-incidence detection (ACD) in emission transaxial reconstruction tomography. The ACD was evaluated in terms of spatial resolution and sensitivity with depth, detection efficiency, effect of pulse-height analysis on resolution and efficiency, correction for attenuation, and cold spot contrast. A prototype positron emission transaxial tomograph (PETT) consisting of a hexagonal array of 24 NaI(Tl) detectors employing ACD was constructed. A fast Fourier transform algorithm was employed to generate the reconstructed image. Computer simulations and phantom and animal studies were carried out to demonstrate that this approach yields tomographic radionuclide images that have high resolution and contrast (hot and cold spot) and that are independent of activity above and below the plane examined. The ACD yields a quantitative nuclear medicine imaging device with high detection efficiency. Comparisons are presented between the ACD and the scintillation camera and scanner. Discussion of the possible applications of the PETT in nuclear medicine is included.

T he recent introduction of the EMI scanner (*1*) has stimulated a great deal of interest in the application of computerized trans-axial reconstruction tomography to diagnostic radiology. EMI employs a high contrast, narrow x-ray beam-scanning technique and removes the superimposition of information with a mathematical algorithm to reconstruct the cross-sectional distribution of attenuation coefficients. EMI's effective use of these techniques has yielded tomographic images of the brain that contain information unattainable by conventional radiographic methods.

Many of the improvements in x-ray transmission imaging demonstrated by EMI are also possible in the field of radionuclide emission imaging. Prior to the introduction of the EMI x-ray scanner, the general principle of transaxial reconstructive tomography had been applied by Kuhl and coworkers (*2–5*) to the reconstruction of radionuclide distributions in the brain. Kuhl's detection method employed a series of rectilinear scans at a number of discrete angles with collimated scintillation detectors of conventional design. This approach has since been applied with modifications by others (*6–11*). Recently, Budinger and Gullberg (*12,13*), Keyes and Simmon

(*14*), and Oppenheim and Harper (*15*) presented results of transaxial tomographic reconstructions that utilized a scintillation camera.

All of the above studies of transaxial radionuclide tomography have employed single photon counting (SPC)* systems such as the scanner and scintillation camera. The work reported here deals with the application of annihilation coincidence detection (ACD)[†] of positron-emitting radionuclides to transaxial reconstruction tomography.

The advantages of ACD in conventional nuclear medicine imaging and transaxial reconstruction tomography have been previously reported by a number of investigators (*16–24*). Brownell and coworkers successfully developed a camera for the imaging of organs containing positron-emitting radionuclides (*18,19*). Their system has also been used to produce transaxial tomographic images (*20,21*). A ring of detectors connected in coincidence was constructed by Robertson, et al (*25*) for use in reconstruction tomography. Cormack (*24*) and Chesler (*20,27*) have discussed some of the advantages of ACD in terms of the criteria of the mathematical reconstruction algorithms.

We evaluated the coincidence detection method in terms of spatial resolution and sensitivity as a function of object depth, effect of pulse-height analysis on resolution and efficiency, correction for attenuation, overall detection efficiency, and cold spot contrast. A prototype positron emission transaxial tomograph (PETT) employing ACD was constructed and the following studies were carried out: (A) computer simulations to evaluate our reconstruction algorithm in the case of ideal detector response and statistics for comparisons to images reconstructed from data taken with the PETT; (B) phantom studies to assess spatial resolution and sensitivity, effect of pulse-height analysis, hot spot, cold spot, quantitative reconstruction, and independence of examined cross section from activity contained in structures above and below the plane of interest (vertical resolution); and (C) animal studies demonstrating the reconstruction of positron-emitting radionuclide distributions in a living animal with and without attenuation corrections.

METHODS

This paper will evaluate the advantages of the ACD method as applied to transaxial reconstruction tomography. We will first consider some of the general assumptions of the mathematical algorithms used as they relate to the method of radionuclide detection. This is

---

---

*Single photon counting (SPC) systems refers to systems that only count individual photons and do not require any time coincidence relationship between multiple photons.

[†]Annihilation coincidence detection (ACD) refers to the simultaneous detection requirement of the two 511-keV photons that are emitted at 180 deg following positron decay.
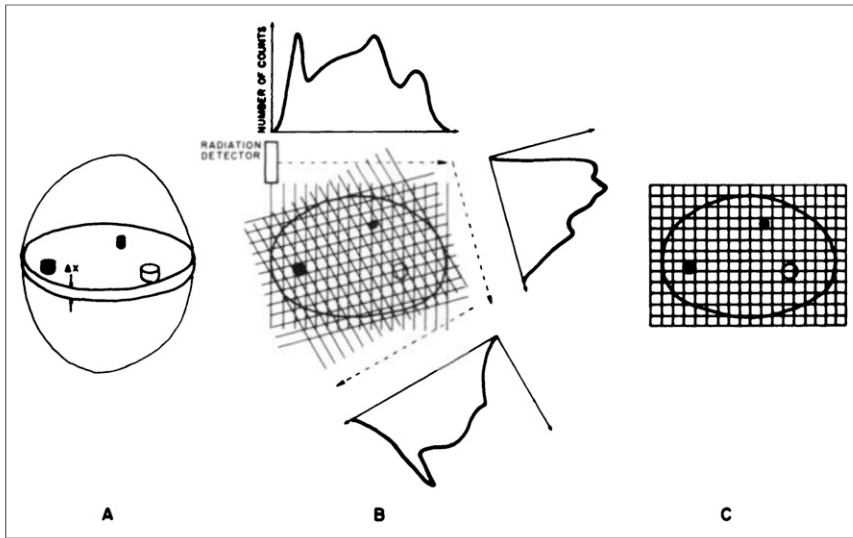
FIGURE 1. (A) Distribution of activity in cross-sectional slice of three-dimensional object. (B) Rectilinear scans performed at number of discrete angles around cross section of interest. Recorded data consists of activity profiles. (C) Reconstructed image formed by using data from activity profiles to mathematically solve for each element in grid or matrix representation.

particularly important since discrepancies between the assumptions of the algorithm and the manner in which the data are collected will result in a distortion of the final reconstructed image.

Reconstruction algorithms

Numerous different reconstruction algorithms have been described for transaxial tomographic section imaging. These algorithms can be broadly classified as Fourier- and non-Fourier-based methods. The Fourier-based algorithms (*24,26–30*) use Fourier transforms, Fourier series, convolutions, or equivalently, filtering of the collected data to perform the reconstruction. Non-Fourier-based reconstruction algorithms (*12,15, 31–33*) in general use algebraic or iterative numerical processing of the data. However, even though there are a number of different types of calculation schemes (algorithms), the general assumptions for the reconstruction are the same.

The purpose of emission transaxial reconstruction tomography is to reproduce the radionuclide distribution in a cross-sectional slice of an object by external detection (Fig. 1A). The data are collected by performing a series of rectilinear scans (or any equivalent linear detection scheme) at a number of discrete angles about the cross section of interest. The data from each rectilinear scan provide an activity profile (Fig. IB) that is used to generate enough "independent" equations to solve mathematically for the unknown distribution of activity in the cross section examined. The unknowns are the individual elements of activity in a grid or matrix (Fig. 1C). Two primary assumptions in the reconstruction algorithms are (A) the cross section is a plane, i.e., it has no thickness ($\Delta X = 0$ in Fig. 1A), and (B) the number of counts recorded at each point along a scan result from the sum of activity in a well-defined line (or region) across the plane of interest. These assumptions imply that the activity distribution in each element of the grid is uniform. For example, the value in each element of the reconstructed image represents the average amount of activity contained in a cube with the dimensions of the linear resolution (grid size) times the thickness of the slice. This would indicate that for maximum resolution and contrast the thickness of the slice should be comparable to the resolution in the rectilinear direction (grid size) since an increase in any one of the dimensions of the cubes reduces resolution and contrast. The second assumption also requires that the detector response have a constant resolution and sensitivity with depth. Thus the detector collimator should be designed with minimum depth-dependent resolution. In addition, a method to compensate for any decrease in sensitivity with depth due to attenuation and geometric efficiency would be required.

Considering the specific requirements of an emission transaxial tomograph and the desired properties of any radionuclide imaging device, the radiation detection system of an emission transaxial tomograph should exhibit the following characteristics: (A) high overall spatial resolution and contrast; (B) depth-independent resolution and sensitivity; (C) facility for an accurate method of performing attenuation corrections; and (D) efficient det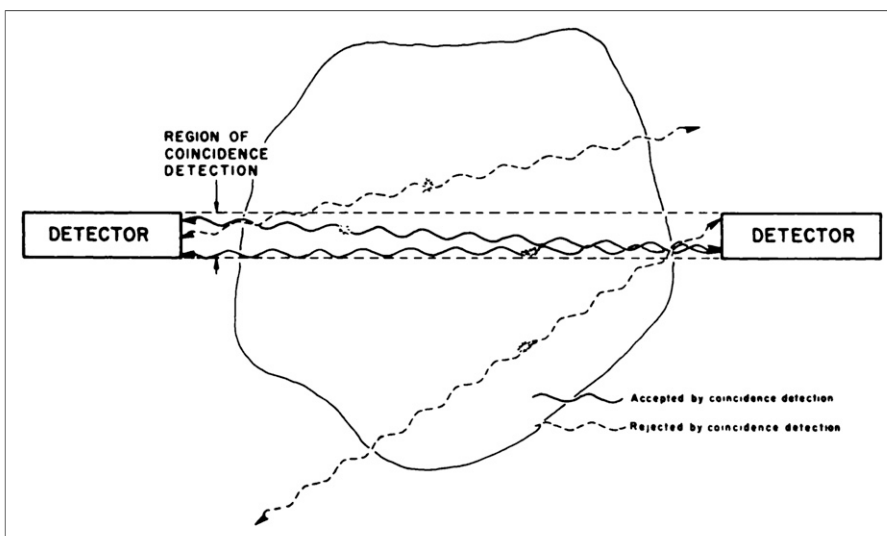ection of the emitted photons. These properties are considered below for ACD, and some comparisons are made with SPC systems.

Coincidence detection of annihilation radiation

In coincidence detection of annihilation radiation, events are recorded when the two 511-keV photons from positron annihilation are detected simultaneously in two detectors. Since the two 511-keV photons are emitted at 180 deg, this limits the field of view to activity lying in a well-defined region between the two detectors. This establishes an "electronic" collimation (Fig. 2) and eliminates the need for the conventional absorption collimators.

Spatial resolution. The line-spread functions (LSF) for a positron-emitting line (⁶⁴Cu) in a water phantom (Fig. 3) centered between two detectors connected in coincidence are shown in Fig. 4. Measurements were taken with two 5.1- × 5.1-cm NaI(Tl)

FIGURE 2. "Electronic" collimation of annihilation coincidence detection. Events are only recorded when two 511-keV photons emitted at 180 deg following positron annihilation are detected simultaneously.

FIGURE 3. Water bath used for measure of line-spread functions, isoresponse, and sensitivity with depth. Water bath was 24 cm long. 20 cm wide, and 10 cm high.

detectors separated by a distance of 54 cm. A single- channel analyzer window was set on the photopeak only (466–555 keV). The 5.1-cm diam NaI(Tl) detectors were shielded with a 2.5-cm thick lead plate with a 2.5-cm straight-bore hole over the center of each detector. This was done to improve the spatial resolution. It is apparent from Fig. 4 that the LSF does not vary significantly over the total distance of 24 cm (full width half maximum, FWHM, varies from 1.1 to 1.2 cm) in a scattering media of water. No collimation is employed other than the "electronic" collimation of coincidence detection, and the resolution is inherent to the exposed detector diameter. The FWHM of the LSF is about 40% of the exposed diameter of the NaI(Tl) detector, as reported by Brownell (18). In contrast, the resolution of detectors with typical absorption collimators used for SPC varies substantially with distance between the detector and the radiation source, as shown in Fig. 5, for an SPC system with a converging collimator. (LSFs for scintillation camera are shown in Fig. 14.)

The effect of accepting lower energy pulses in ACD is demonstrated in Fig. 6 in which the LSFs with photopeak only and with pulses from 100 keV and above are shown. The FWHM resolution is increased slightly in the latter case, but at the full width tenth maximum (FW 0.1M) there is an increase of about a factor of 3 due to the acceptance of scattered radiation. It is important to note that when only the photopeak is used, 75% of the total counts fall within the resolution of the FWHM, but when 100 keV and above is used, 55% of the pulses occur outside the FWHM and range over a large lateral distance (approximately 9 cm, Fig. 6). The advantage of accepting all the pulses above 100 keV as compared with only the photopeak is that the detection efficiency is greatly increased since many of the low-energy events result from partial interactions in the detector of 511-keV photons.

Some degree of uniformity in the isosensitivity response of SPC can be achieved by suitably designed collimators (34–36), by summing or by taking the geometric mean of the response of two opposing detectors. The latter tends to improve the uniformity of response by decreasing the resolution at positions of high resolution, and vice versa. Nevertheless, as pointed out by others (16,17,23,37), SPC does not achieve the uniformity of response provided by coincidence detection of annihilation radiation.

Depth-independent sensitivity. Coincidence detection of annihilation radiation provides a means of detecting radionuclides with a depth-independent sensitivity. Figure 7 is a plot of the integrated LSFs (from Fig. 4) at the various depths in the water phantom. (The integral of the LSF is equivalent to a plane source response.) The constant counting rate and sensitivity are due to the fact that the attenuation and solid angle efficiency are constant. The depth-independent attenuation results from the fact that the two 511-keV annihilation photons must always cross a total path length, D, to be detected in coincidence (Fig. 3). For example, if one 511-keV photon traverses a short distance of a, the other must traverse the long distance of b. Thus the attenuation of the annihilation radiation is only a function of the total length, D, independent of the depth of its origin. The solid-angle efficiency is also constant as a function of depth because it results from the combined efficiency of two coincidence detectors and at different depths as the solid angle for one detector increases, the other decreases (18). Therefore the absolute sensitivity can be calculated from the total path length, D, and the attenuation coefficient of the total material traversed. This is not the case with SPC, in which the response decreases with depth due to the increasing path length through

FIGURE 4. Line-spread functions, LSFs, for positron-emitting line source (⁶⁴Cu) in water phantom (Fig. 3) centered between two detectors connected in coincidence. Only photopeak was used. Values of FWHM resolution are given in centimeters.
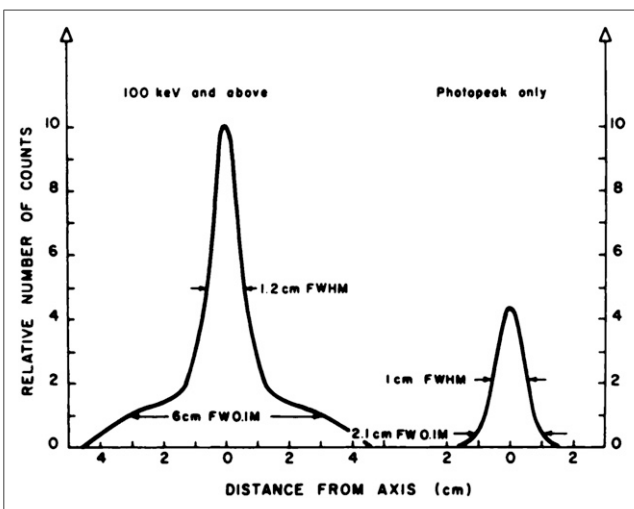
FIGURE 5. Line-spread function in water from SPC system. Detector system consisted of 2.5-cm diam X 5-cm thick NaI(Tl) and Ohio-Nuclear converging collimator No. 55035-L shielded down to 2.5-cm diam detector (interior 7 holes open). Collimator focal length was 12.7 cm; distance between collimator and water phantom was 4 cm.

the object and the corresponding increase in attenuation. Furthermore, the variation in geometric response of conventional absorption collimators compounds the difficulty in defining the origin of the detected photons for attenuation correction. The higher energy of the 511-keV photons also decreases the undesirable variations that occur when tissues of varying composition and thickness are traversed.

Efficiency. The directional or positional information obtained with SPC systems is fundamentally different from the "electronic" collimation of ACD. The directional information from a SPC system is obtained by limiting the detector field of view with an absorption collimator. The photons stopped by the collimator are lost to the image, which sets theoretical limits on efficiency. With coincidence detection of annihilation radiation, absorption collimators are not

necessary, and as discussed by Burnham and Brownell (*19*), all the radiation emitted could be detected and its origin established (neglecting attenuation in the object).

The efficiency of multiple detectors with single photon counting increases linearly as the number of detectors is increased whereas ACD systems composed of multiple detectors can be designed to increase efficiency by the square of the number of detectors. This can be illustrated by comparing an SPC system with an ACD system, each composed of two detectors. If the number of detectors is increased from two to four, the SPC system efficiency will increase by a factor of 2 whereas the ACD system efficiency will increase by a factor of 4 (Fig. 8). This can be generalized for multiple detector arrays by the following equation:*

$$R_C/R_g = KN^2/N = KN \qquad (1)$$

where R_c, R_g, and N are the coincidence counting rate, single photon counting rate, and numbers of pairs of detectors, respectively. The term K is the proportionality constant, which can be determined by measuring the coincidence to single photon counting rate for a single pair of detectors. To evaluate K, a cylinder of activity, either 2.2 or 1.1 cm in diameter and 20 cm long, was placed between a pair of collimated SPC detectors (same collimators as used in Fig. 5) and ACD detectors. The detector diameters of 5.1 and 2.5 cm were used for the 2.2- and 1.1-cm diameter cylinders of activity, respectively. The counting rates from these systems were normalized to the number of millicuries. (The number of millicuries of ^{64}Cu represents a pure positron emitter.) The results of these comparisons are shown in Table 1. The ratio R_c/R_g was found to be about 0.12 when only the photopeak was used in ACD and increased to about 0.26 if a lower level discriminator was set to accept all the pulses from 1,000 keV and above.

A cylinder of activity was chosen for a comparison of efficiency between SPC and ACD systems since in the specific case of transaxial reconstruction tomography the activity is assumed to be in a uniform region between the detectors. Although the SPC collimator used in this work may not be of optimal design, it represents a reasonable approximation of the total efficiency for detection of the activity in the cylinders. In fact, a better collimator design for a more uniform resolution with depth would probably result in a lower efficiency for the SPC system.

Using the values of K listed in Table 1, the ratio of R_c/R_g versus the number of detector pairs is plotted in Fig. 9. It is seen that with the photopeak and 100-keV discriminator settings for ACD, the ratio of R_c/R_g is unity at eight and four pairs of detectors, and as the detectors pairs are further increased, the ACD rapidly dominates in efficiency. The line in Fig. 9 with K = 0.5 is considered an upper limit, taking into account an optimal resolution design of SPC and increases in coincidence efficiency resulting from thicker detectors than those used in this work (5.1 cm thick). Thus, previous conclusions regarding

FIGURE 6. Line-spread function in water for ACD comparing difference between accepting energies of 100 keV and above to photopeak only. FWHM and FW 0.1 M are shown.

---

*Equation I assumes that the coincidence efficiency is constant for all of the detector pairs. However, as the angle increases between the detectors, the distance between detectors will increase by the 1/cosine of the angle. In most cases, this angle will vary from 0 to 20 deg and even at the worst case of 20 deg the increase in distance is only a factor of 1/cos2odeg = 1.06.
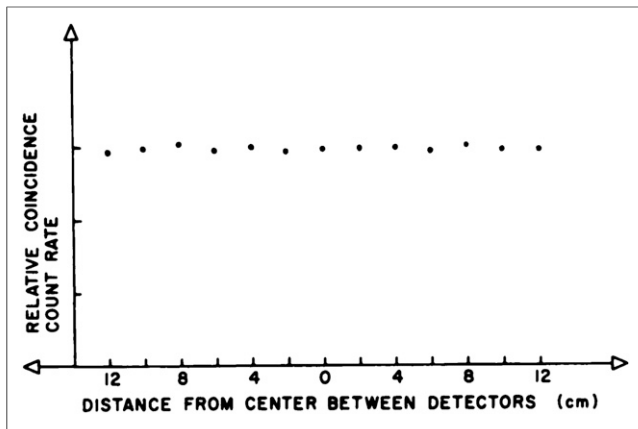
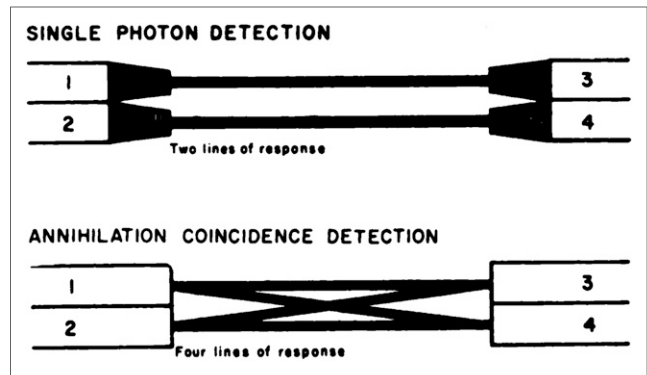**FIGURE 7.** Plot of integrated line-spread function response to show depth-independent sensitivity of ACD.

FIGURE 8. Illustration of N and N² dependence of efficiency for SPC and ACD, respectively, for multiple detector arrays. N is number of detector pairs.

comparisons of efficiency between dual-probe scanners with SPC and ACD (*23,38*) do not apply in the case of larger arrays of detectors using this multiple coincidence scheme.

Cold spot contrast. Cold spot imaging is one of the most difficult tasks in nuclear medicine because of the low inherent contrast and degradation of contrast from the contribution of scattered radiation. Cold spot detection capabilities of a single-probe scanner and camera with ^{99m}Tc and an ACD with ^{64}Cu were compared. The phantom consisted of a water bath (18 cm × 10 cm × 10 cm) filled with the appropriate activities and a 2.3-cm diam plastic rod scanned across the phantom at different depths.

If one assumed that the spatial resolution of an ideal detection system was 1.1 cm and constant with depth, the predicted maximum decrease in counting rate without any degradation due to scatter would

be about 13%. It can be seen in Fig. 10 that the contrast of the ACD system essentially agrees with the ideal without any loss in contrast with depth. However, both the scanner and camera showed an exaggerated contrast at the surface due to their inherent loss in sensitivity with depth and then contrast rapidly diminished to zero with depth.

The protoype PETT

To evaluate the ACD method for emission transaxial reconstruction tomography, a prototype system was designed, constructed, and tested. This system is referred to as a positron emission transaxial tomograph (PETT). A schematic illustration and photograph of this system are shown in Figs. 11 and 12.

The detection system consists of 24 5.1- × 5.1-cm NaI(Tl) scintillation detectors placed in a hexagonal array (four to a side). Lead shields 2.5-cm thick with 2.5-cm diam straight-bore holes are placed

TABLE 1
Comparison of Detection Efficiency of SPC and ACD for a Single Pair OF Detectors*

Diameter of cylinder of activity (cm)	Collimation	Detector diameter (cm)	Pulse-height selection	Efficiency (cps/mCi)	Ratio of coincidence to single photon counting (k)‡
Single photon counting (^{99m}Tc)					
2.2	none	5.0	photopeak	113,700	–
2.2	Ohio-Nuclear†	5.0	photopeak	30,300	–
1.1	none	2.5	photopeak	41,942	–
1.1	Ohio-Nuclear†	2.5	photopeak	9,025	–
Coincidence counting (^{64}Cu)					
2.2	none	5.0	photopeak	93,542	–
2.2	coincidence	5.0	photopeak	3,592	0.12
2.2	none	5.0	100 kev and above	292,891	–
2.2	coincidence	5.0	100 kev and above	8,931	0.29
1.1	none	2.5	photopeak	29,716	–
1.1	coincidence	2.5	photopeak	1,016	0.11
1.1	none	2.5	100 kev and above	102,181	–
1.1	coincidence	2.5	100 kev and above	2,107	0.23

*Detector separation distance was 45 cm and cylinder of activity was 20 cm long.
†Ohio-Nuclear collimator no. 55035-L, resolution of 1.3 and 1.1 cm at focal point with 5-cm and 2.5-cm defector, respectively.
‡The value of K refers to the coincidence and SPC collimated systems with the corresponding cylinder of activity.
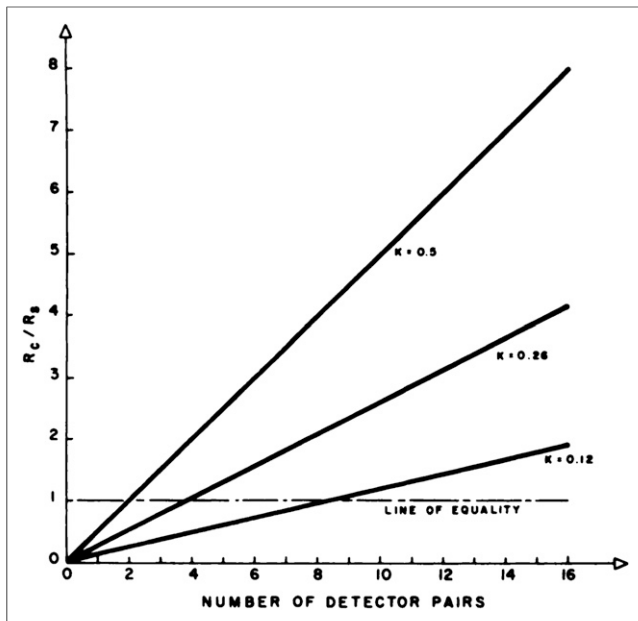
FIGURE 9. Plot of ratio of annihilation coincidence, R_c, to single photon, R_a, counting rates versus number of detector pairs, N. K is ratio of R_c to R_a for single pair of detectors. K = 0.12 and 0.26 are values for SPC system described in text to ACD system with photopeak only and 100 keV and above, respectively. K = 0.5 is given as a possible upper limit for optimal design for two systems. Line of identity indicates number of detector pairs required for systems to have equal efficiency.

in front of each detector to increase the inherent detector resolution to about 1.1 cm FWHM, as shown in Fig. 4. Lead shielding is provided to exclude radiation originating outside the cross section examined. The output of each detector is connected to individual preamplifiers, amplifiers, and single-channel pulse-height analyzers. The single-channel pulse-height analyzer output of each set of directly opposing detectors is connected to a coincidence circuit with a resolving time of 30 nsec (Fig. 11). This establishes the "electronic" collimation of the 12 sets of detectors. With the above resolving time and shielding, the random coincidence rate of the data collected in this work for the highest single detector counting rate (12,000 cps) was less than 5% of the true coincidence rate. The outputs of the 12 coincidence units are routed into a parallel channel interface to an Interdata Model 70 minicomputer.

In the prototype PETT, the object examined is placed in the center of the 24-detector hexagonal array on a platform that is rotated under computer control (Fig. 12). Coincident data from the 12 coincident pairs of detectors are recorded every 7.5 deg through a full 360-deg rotation of the object under study. As a result of the offset positions of the opposing banks of detectors ($\Delta_1, \Delta_2, \Delta_3$) (Fig. 11), there are 24 data points with a sampling resolution of 1 cm in the transverse direction at every 7.5 deg after completion of the 360-deg rotation of the object.*

This data is stored, sorted, and then processed by a Fourier-based reconstruction algorithm using the Interdata Model 70 minicomputer. The algorithm used in this work was developed by the Biomedical Computer Laboratory at Washington University School of Medicine and employs fast Fourier transforms in the back projection of filtered projections at each discrete angle. The successive projections are summed to generate the reconstructed image. The data-processing time

for a 24 X 24 array of the Fourier transform reconstruction algorithm is about 25 sec with programs written in FORTRAN. The Interdata assembly language version of the algorithm would shorten the processing time.

Computer simulation. The reconstruction algorithm used in this study was evaluated by performing reconstructions of computer-simulated phantom data (ideal statistics) with the same linear and angular sampling as used with the PETT. The simulated phantom is drawn on the numerical printout of Fig. 13, and the reconstructed image is shown in the lower portion of the same figure. The numerical values are in good agreement with the actual values of the activities in the cylinder, the 2-cm diam hot region, and the 3-cm cold region. However, the values for the 1-cm thick ring and 1-cm diam hot region of about 180 and 330 are lower than the correct values of 300 and 500. This is explained by the fact that the sampling resolution, ring, and hot region dimensions are all 1 cm and from the sampling theorem (*39*) the exact answer can only be recovered if the sampling resolution is less than or equal to one half the object size.*

Attenuation correction. Although the attenuation of radiation is constant with respect to depth between two detectors in annihilation coincidence, varying thicknesses of material are interposed between each detector pair as data are collected at different points across the object. Thus an attenuation correction must be made on each data point recorded. One method is to determine the physical dimensions of the object and multiply each data point by $e^{\mu x}$, where x is the thickness of the object between the coincidence detector pairs and μ is an average linear attenuation coefficient. This approach is subject to error if an accurate value of μ is not known as in cases where varying thicknesses of lung or bone are traversed. Another method consists of measuring the attenuation of 511-keV radiation in the subject and then using this information to correct the emission data before reconstruction. We have used the former method in the phantom studies. However, the latter method was used in the animal studies by placing a thin plastic ring containing a solution of ^{64}Cu around the subject and collecting coincidence data as a function of transverse and angular position. The same measurement was made without the subject in position and the ratio of the two measurements gives the attenuation factor. Because of the well-defined and depth-independent response of annihilation coincidence, this attenuation correction method is accurate and simple to implement.

RESULTS

Phantom studies

Spatial resolution. To evaluate the overall resolution and the effect of pulse-height analysis of the PETT, three capillary tubes, 2.0 mm in diameter, containing a solution of ^{64}Cu were placed in an 18-cm diam cylindrical phantom filled with water (Fig. 14). Data were collected with the PETT using only the photopeak and then accepting pulses from 100 keV and above. The reconstructed images contained 200,000 counts (Fig. 14). The LSFs were constructed from the numerical printout (Fig. 14, bottom). For comparison, the same phantom containing ^{99m}Tc was placed against the face of a Searle Radiographics HP scintillation camera fitted with a high-resolution 15,000-hole collimator. The phantom was oriented such that the line sources formed an angle of 60 deg with respect to the face of the camera. The projected distance between the line source was 4.8 cm. The line sources were 2, 9, and 16 cm from the face of the camera and 200,000 counts were collected.

---

*The prototype PETT is more completely described by Ter-Pogossian MM, Phelps ME, Hoffman El, et al: A positron emission tomograph for nuclear medicine imaging (PETT). *Radiology*: to be published.

---

*The sampling theorem states that the sampling resolution must be less than or equal to one half the object size for quantitative recovery. Experimentally, the necessary sampling resolution is usually from one half to one fourth the object size if quantitative recovery is to be expected.
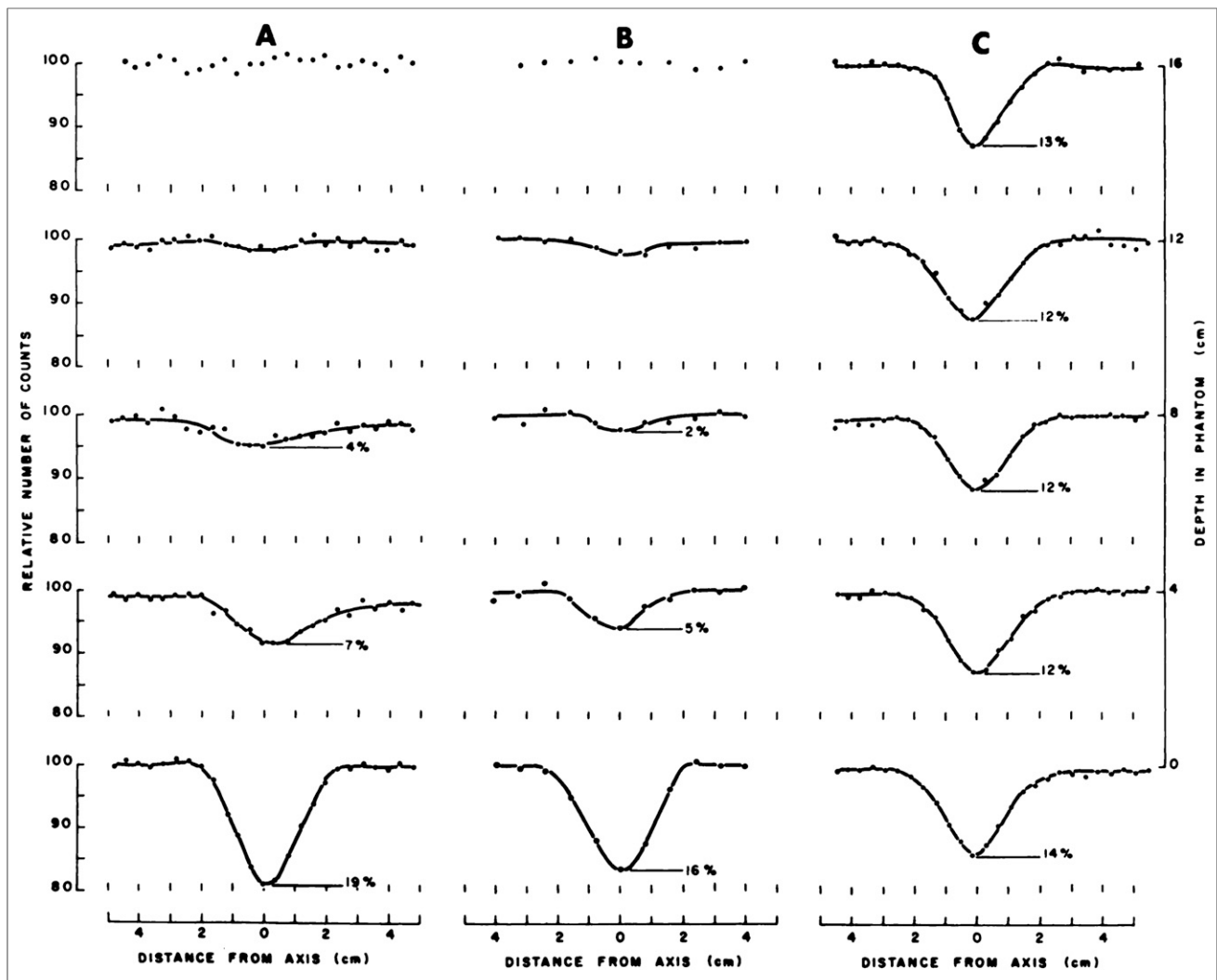
FIGURE 10. Comparison of cold spot scanning with 2.2-cm diam rod in water phantom containing either ^{99m}Tc or ^{64}Cu, for (A) scanner with absorption converging collimator (same counting system as used in Fig.5, collimator-to-water bath distance 6 cm), (B) scintillation camera with 15,000-hole high-resolution collimator with water phantom placed against surface of collimator, and (C) annihilation coincidence system used for LSFs measurements in Fig. 4. Approximately same amount of activity and counting times were used in all cases.

Numerical data from the scintillation camera were used to construct the LSFs shown in Fig. 14. This illustrates the decrease in resolution and sensitivity with distance for the scintillation camera and depth-independent resolution and sensitivity of the PETT. It can also be seen from Fig. 4 and Fig. 14 that the LSFs for the detector response and the PETT system (including reconstruction) do not differ significantly when only the photopeak is employed. However, when energies of 100 keV and above are used, a significant change is observed. The individual detector LSF had a FWHM of 1.2 cm and FW 0.1M of 6 cm (Fig. 6). After processing in the reconstruction algorithm, the FWHM was 1.4 cm but the FW 0.1M is reduced from about 6 cm to 3 cm. This is a result of the reconstruction algorithm, which in effect has diminished the low-frequency components which comprise the detector LSFs due to the acceptance of scattered radiation. The PETT LSFs from the reconstructed image with photopeak only are much more uniform and of higher resolution than the 100 keV and above case but the difference is less marked than for the actual detector LSFs.

The independence of the cross-sectional slices in the vertical direction (vertical resolution) was evaluated by constructing a phantom that had two separate sections (Fig. 15). The lower section contained a ring of activity surrounding a uniform cylinder of activity. The upper section, which was 6 mm from the center of the lower section, contained a ring of activity and a cylinder of activity containing two 2-cm diam hot sections and a 3-cm diam cold section. Data were collected separately from both sections with the PETT and the reconstructed images are shown in Fig. 15. The image from the lower section (right side of Fig. 15) does not show the structure of the section immediately above it even though the structure in the upper section was only 6 mm from the center of the lower section.

Quantitative and cold spot images. The ability of the PETT to yield quantitative images was tested with a phantom filled with relative positron activities of 1, 4, and 0 in a 14-cm diam cylinder and two 3-cm diam tubes, respectively (Fig. 16). The reconstructed activities were 1 ± 0.1, 4 ± 0.1, and 0 ± 0.1 in the cylinder and two 3-cm diam tubes, which is in excellent agreement with the relative
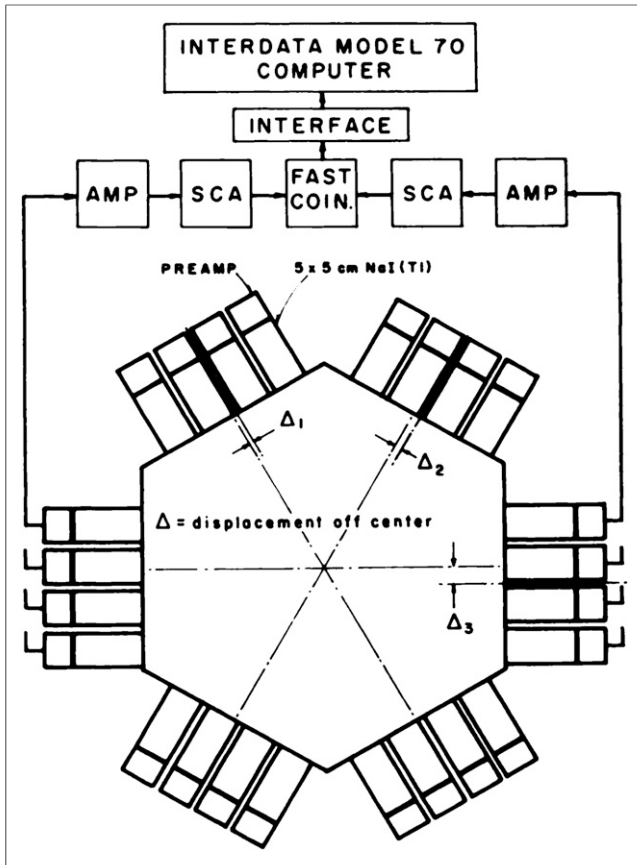
FIGURE 11. Schematic illustration of prototype PETT.

activities in the phantom and consistent with the statistical accuracy of the data. The 3-cm diam objects were employed to demonstrate the quantitative aspect of the reconstruction since the sampling resolution (approximately 1.0 cm FWHM) must be less than or equal to two times smaller than the object size for quantitative reconstruction in accordance with the sampling theorem.
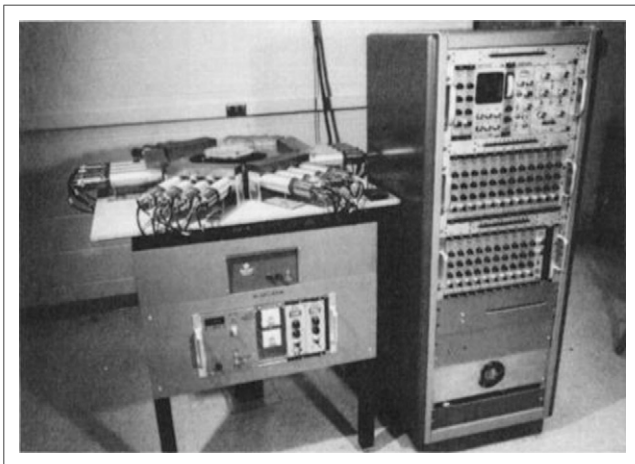

FIGURE 12. Photograph of prototype PETT. Object examined (phantom or animal) is placed on computer-controlled turntable at center of hexagon. Axis of rotation is perpendicular to plane of hexagon. Phantom is shown on turntable.

To evaluate the cold spot reconstruction with the PETT, a 14-cm diam phantom was filled with ^{64}Cu and voids (tubes filled with water) ranging from 1 to 3.5 cm in diameter were placed in the phantom (Fig. 16). All the voids are visible in the reconstructed image and the actual level of activity in the void from the reconstructed image is zero, except for the 1-cm void, which cannot be recovered fully in accordance with the sampling theorem as discussed before.

Comparison of the PETT and scintillation camera. In a comparison of the imaging capabilities of the PETT and the scintillation camera used in a conventional mode (no tomography), the phantom shown schematically in Fig. 17 was filled with an equal number of microcuries of ^{64}Cu and ^{99m}Tc, respectively, and images containing 300,000 total counts were recorded. The phantom was 18 cm in diameter and 6 cm high. Data collection time for the PETT to record 300,000 counts from a 1-cm thick cross-sectional slice of the phantom was 12 min, whereas the camera required 16 min to collect 300,000 counts from the entire phantom. The reconstructed image from the PETT gave an excellent reproduction of the cross-sectional distribution of activity in the phantom whereas the identification of the activity distribution in the phantom was ambiguous from the camera image.

A comparison of data collection times between the PETT and scintillation camera for several different types was done to indicate the general efficiency of the prototype PETT (Table 2). Equivalent activities of ^{64}Cu and ^{99m}Tc were employed for the PETT and the camera and in all cases the time and number of counts refer to an approximately 1-cm thick cross section for the PETT image and to a total 6-cm high phantom for the camera image.
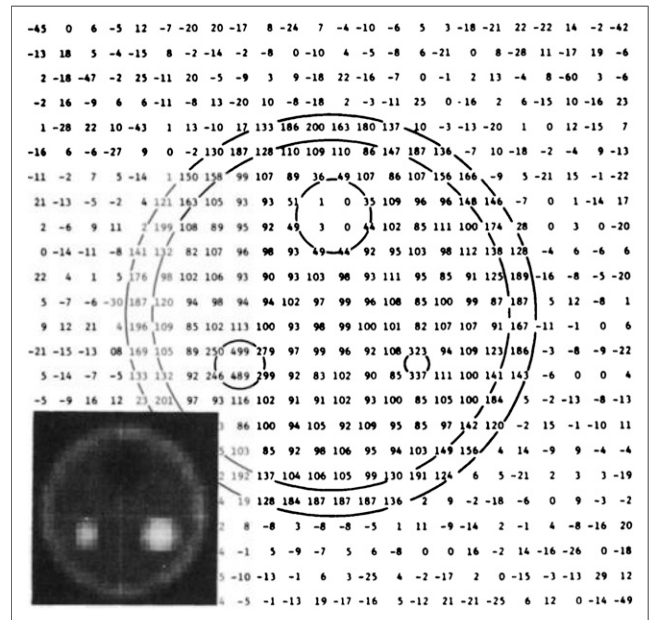

FIGURE 13. Computer simulation to evaluate Fourier transform reconstruction algorithm, 1-cm linear sampling resolution and *7.5 deg*-angular sampling employed in PETT studies. Actual phantom is drawn on numerical printout with reconstructed image at bottom left-hand corner (image has right-to-left inversion from numerical printout). Actual values in 1-cm thick ring, 14-cm cylinder, 2-cm and 1-cm hot regions, and cold region were 300, 100, 500, 500, and 0, respectively.
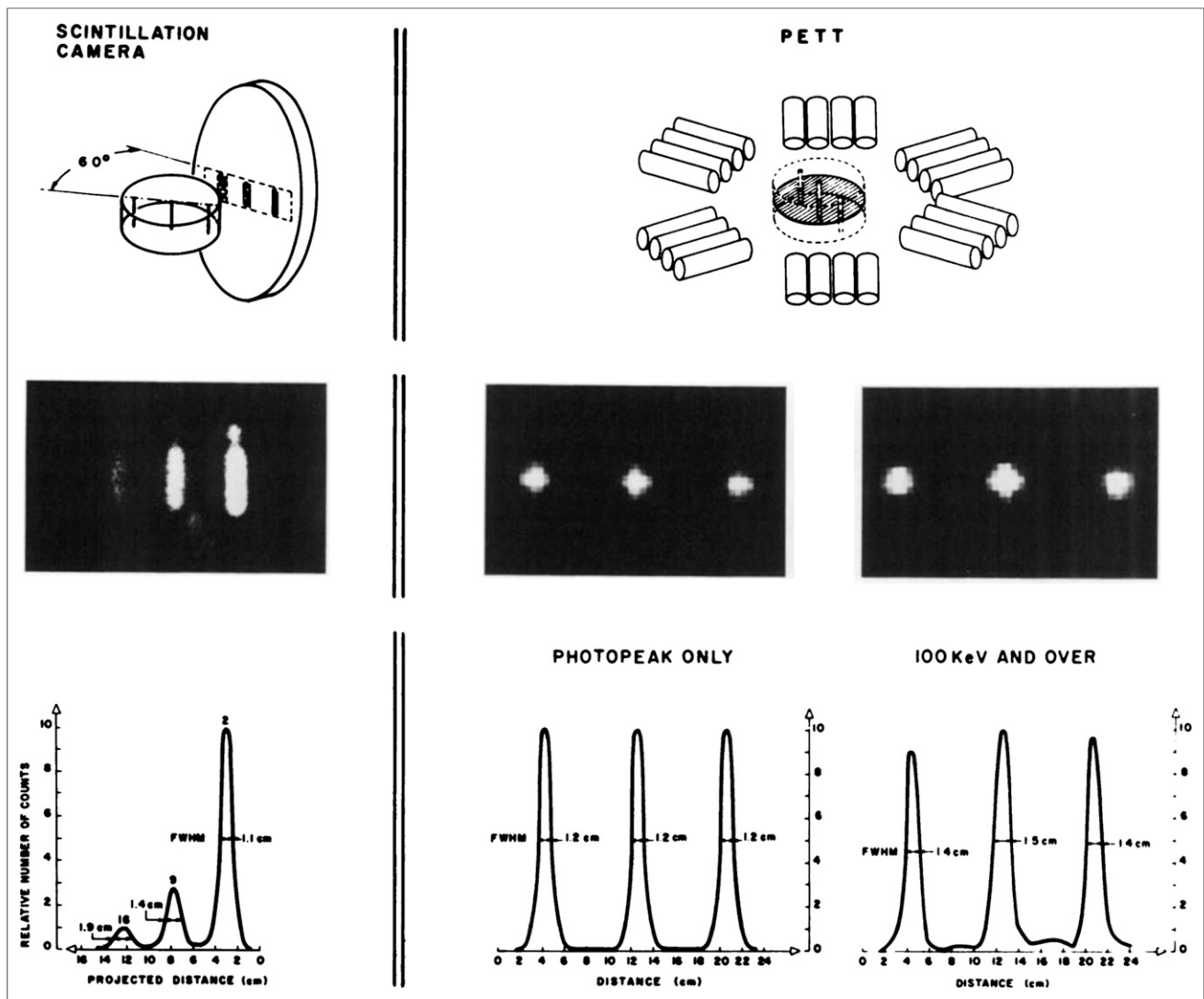
FIGURE 14. Comparison of line-spread functions for scintillation camera, 20% symmetrical energy window, and PETT accepting photopeak events only and 100 keV and above. Top: diagram of placement of phantom. Middle: recorded images. Bottom: line-spread functions. Technetium-99m and ^{64}Cu were used for camera and PETT, respectively.

Animal studies

A study was carried out to assess the capabilities of the PETT for organ visualization by means of intravenously administered pharmaceuticals labeled with positron-emitting radionuclides and to demonstrate the importance of proper attenuation corrections. An anesthetized dog (23 kg) was placed on the rotating table in the center of the PETT. Following the administration of a positron-labeled radiopharmaceutical, data were collected every 7.5 deg for a 360-deg rotation.

The 1-cm thick cross section examined was at the level of the sixth thoracic vertebra. The experiment was carried out in the following sequence: (A) the dog was intravenously injected with 10 mCi of $H_2{}^{15}O$ (^{15}O, $t_{1/2}$ = 2 min) (40). Three minutes was allowed for equilibration with the fast equilibrating water compartments and data were collected for the ensuing 4.8 min. (B) Twelve millicuries of $^{13}NH_3$ (^{13}N, $t_{1/2}$ = 10 min) (41) were injected intravenously and 8 min allowed for the clearance of the ammonia from the blood and equilibration in soft tissues. Data collection period was 12 min. (C) The dog was allowed to breathe ^{11}CO (^{11}C,

$t_{1/2}$ = 20.4) (42) for about 1 min to label the blood with approximately 9 mCi of ^{11}CO-hemoglobin. Five minutes was allowed for equilibration in the blood pool before a 24-min data collection period.

The anatomical structures (Fig. 18) were identified by A-P and lateral x-ray films and by autopsy. The reconstructed images shown at the top of Fig. 18 were corrected for attenuation by the transmission method described in the Methods section. The transmission data were also processed in the reconstruction algorithm and the resulting transmission image is shown in the bottom left-hand corner of Fig. 18. The image taken with $H_2{}^{15}O$ shows the distribution of equilibrated water in soft tissue. The equilibration of bone water is slow which accounts for a void in the image at the position of the vertebral column.

The lungs also show a relatively low concentration of $H_2{}^{15}O$. The $^{13}NH_3$ is preferentially taken up in the myocardium as reported by others (43,44). The image contrast between the myocardium and the surrounding soft tissue is about 8 to 1. The ^{11}CO- hemoglobin image demonstrates the blood distribution to the chambers
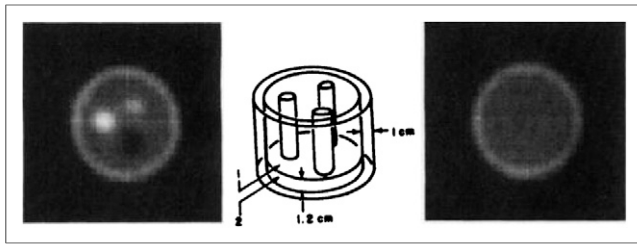
FIGURE 15. Evaluation of interference in reconstructed image taken with PETT from activity above level of interest. Center: schematic of split level phantom. Left: image taken at level 1 containing relative activities of 3, 1, 5, 3, and 0 in 1-cm ring, 14-cm cylinder, two 2-cm hot regions, and 3-cm cold region. Right: image taken from level 2 which contained only 1-cm ring and 14-cm cylinder and was 6 mm from center of level to above structure.

in the heart, the large blood vessels, and the general blood distribution in the surrounding tissues.

The $H_2^{15}O$, $^{13}NH_3$, and ^{11}CO images in the lower portion of Fig. 18 have not been corrected for attenuation and illustrate the resultant distortion.

The images mentioned above were recorded without any phasic data collection with respect to cardiac cycle or respiration.

DISCUSSION

The evaluations carried out in the Methods section on ACD and the studies applying this technique to transaxial reconstruction tomography with the prototype PETT in the Results section demonstrate that this system meets the stringent criteria of emission
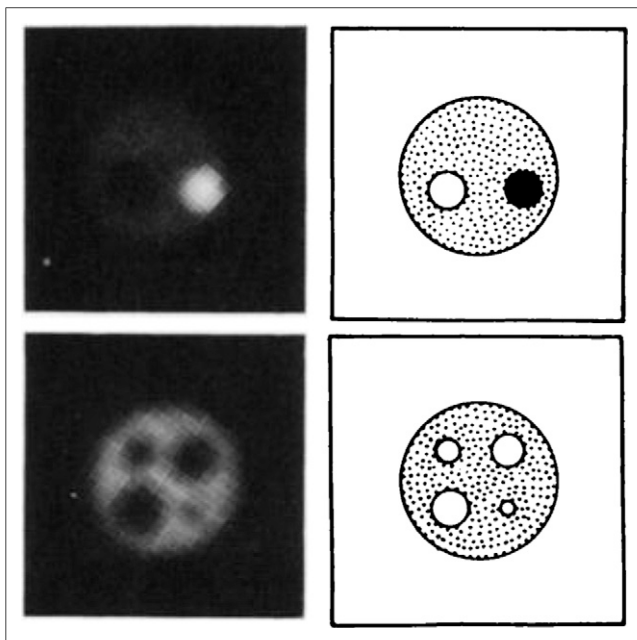

FIGURE 16. Top: test of quantitative reconstruction with PETT. Phantom consisted of 14-cm cylinder, 3-cm hot region, and 3-cm cold region with relative activities of 1, 4, and 0. Values in reconstructed images are 1 ± 0.1, 4 ± 0.1, and 0 ± 0.1. Image contained 340,000 counts. Bottom: test of cold spot reconstruction with PETT. Phantom consisted of 14-cm diam cylinder of activity with 3.5, 3, 2, and 1-cm voids (tubes filled with H_2O). Image contained 300,000 total counts.

transaxial reconstruction tomography. The ACD of the PETT provides a method of detection with the following properties: (A) high spatial resolution that is a function of the exposed detector diameter (FWHM of LSF is approximately 40% of exposed detector); (B) resolution and sensitivity are essentially depth independent as compared with conventional absorption collimator detector systems that exhibit a depth-varying response due to varying geometric efficiency and attenuation; (C) attenuation correction in the reconstructed image is simple and accurate for the ACD system due to the depth independence of sensitivity and resolution. The attenuation correction schemes necessary for SPC systems must take into account both the depth-dependent sensitivity and the geometric variations of the collimated field of view. Even if proper attenuation corrections are possible in single photon-counting systems, the lower contrast ratio of deep-seated structures requires a large attenuation correction applied to less well-defined structures. The approximations used to correct for these factors, or ignoring them, results in a distortion of the image (Fig. 18). The magnitude of these distortions and their significance in the reconstructed images have not yet been fully investigated, (D) The ACD method provides a high overall contrast for cold and hot spots.

The lateral dimensions of the phantoms and animals studied in this work did not exceed 20 cm because of the limited field of view of the prototype PETT. However, ACD can be applied to considerably larger objects without a significant loss in the quality of the properties mentioned above. This is in contrast to SPC techniques in which the quality of the detection system decreases as the object size increases.

The positron emission transaxial tomograph can be designed to utilize the radiation emitted by radionuclides more efficiently than is generally possible with SPC systems. The prototype PETT used in this work employed only the coincidence between directly opposing pairs of detectors. However, as discussed in the Methods section, a much more efficient utilization of the annihilation radiation is accomplished by the use of a multiple coincidence logic (Fig. 8). This type of logic for a 24-detector prototype PETT (Fig. 19) would increase the number of coincidence outputs from 12 to 48, an increase in efficiency of approximately a factor of 4. We are presently constructing a system with eight detectors per side (48 detectors total) with 192 pairs of detectors in coincidence. This system will be large enough for both human head and torso. Since the prototype PETT has an efficiency comparable to the scintillation camera (Table 2 and Fig. 17), and since this efficiency
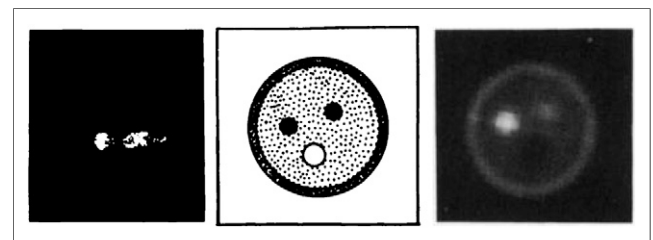
FIGURE 17. Comparision of images containing 300,000 count recorded with PETT and scintillation camera. Phantom is shown schematically in center. Ring (1 cm), 14-cm cylinder, two 2-cm hot regions, and 3-cm cold region contained relative activities of 3, 1, 5, 3, and 0. Technetium-99m and ^{64}Cu were employed for camera and PETT, respectively. Phantom was placed against face of 15,000-hole high-resolution collimator of camera.

TABLE 2
Comparison of Data Collection Times of Scintillation Camera* and PETT Scanner

Phantom[†]	Total activity[‡] (μCi)	Total number of counts in image	Data collection time (min) Scintillation camera	PETT
17-cm diam cylinder (1), 3-cm diam tube (0)	370	280,000	15	12
1-cm thick ring with 17-cm diam (3), 14-cm diam inner cylinder (1), 3-cm tube (0), 2-cm diam tube (10)	600	440,000	16	12
1-cm thick ring with 17-cm diam (2), 14-cm diam inner cylinder (1), 3-cm diam tube (0), 2-cm diam tube (4)	480	350,000	14	12

*Searle Radiographics Model HP fitted with 15,000-hole high-resolution collimator.

[†]Phantom consists of a Lucite cylinder approximately 18 cm external diameter and 6 cm high filled with a solution of either ^{99m}Tc or ^{64}Cu. Various cylindrical containers with different activities are placed in the phantom. Numbers in parentheses refer to the relative activities.

[‡]^{99m}Tc for the scintillation camera and ^{64}Cu for the PETT.

can be increased by using the multiple coincidence design shown in Fig. 19 (see also Fig. 9), the newer device should provide tomographic imaging capabilities with a greater efficiency than conventional systems employed in nuclear medicine.

The quantitative imaging capability of the PETT provides a means for carrying out accurate determinations of physiologic variables with appropriate radiopharmaceuticals. In addition, in terms of image quality, the quantitative capabilities of the system result in an image contrast that is equal to the object contrast. For example, if the target-to-nontarget activity ratio is 15:1, then the image contrast will also be 15:1 for object sizes with equal to or greater than twice the resolution of the tomograph (see Results section and Fig 16).

It is significant that the low resolution components of the broad detector LSFs that occur when the energy discrimination is lowered to 100 keV (Fig. 6) is improved in the tomographic reconstruction (Fig. 14). This demonstrates that the data processing in the algorithm can effectively remove some of the deleterious effects of scatter in the reconstructed image. It should be pointed out, however, that if the loss in contrast from the detector response is so large that the objects are poorly detected or not detected at all, the algorithm will not be effective in removing the effects of scattered radiation (what you can't detect, you can't reconstruct).

The significance of the processing with the reconstruction algorithm in the EMI scanner is appreciated by most investigators but equally important is the fact that the high-contrast narrow-beam scanning technique allows the detection of attenuation that was not perceptible by conventional radiographic techniques. We feel that this same advantage in radionuclide imaging is possible with the ACD technique employed in the PETT. In addition, the general feature of transaxial reconstruction tomography that results in a cross-sectional image with the removal of the superimposition of information is also a significant factor in improving nuclear medicine imaging.

The fact that the PETT is limited to positron-emitting radionuclides may appear to limit the usefulness of this technique in clinical nuclear medicine. There are a number of positron-emitting radionuclides, however, with favorable physical and chemical properties for their application in nuclear medicine. Gallium-68 ($t_{1/2}$ = 68 min) is produced by a commercially available long-lived generator, ^{68}Ge ($t_{1/2}$ = 272 days) and is a positron-emitting analog to ^{67}Ga, the usefulness of which is well recognized in nuclear medicine. In addition, ^{68}Ga could be utilized in a number of other existing nuclear medicine procedures. For example, ^{68}Ga-DTPA
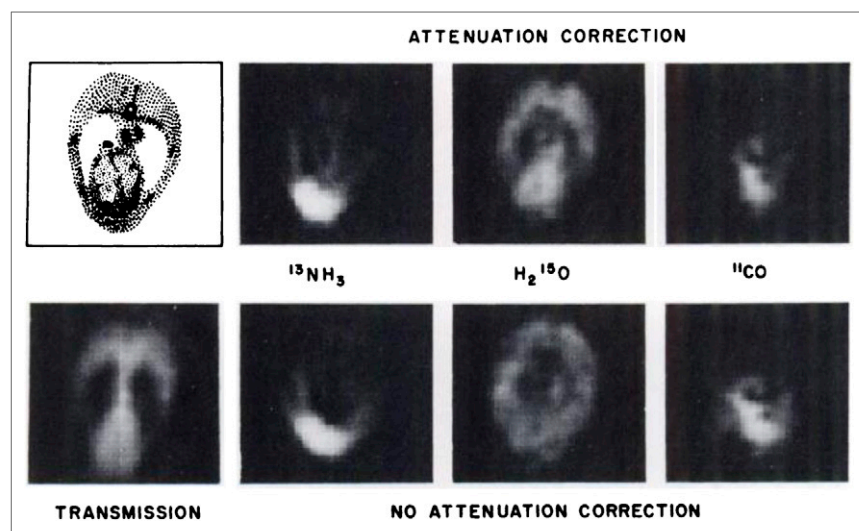
FIGURE 18. Reconstructed imges from 1-cm thick cross section of dog at level of sixth thoracic vertebra following intravenous administration of H$_2$^{15}O, ^{13}NH$_3$, and ^{11}CO. Corresponding images contained 63,000, 230,000, and 350,000 counts. Sketch of anatomic structure at this level is shown at top left. Reconstructed transmission image is shown at lower left. Reconstructed images on top were corrected for attenuation; those on bottom were not.
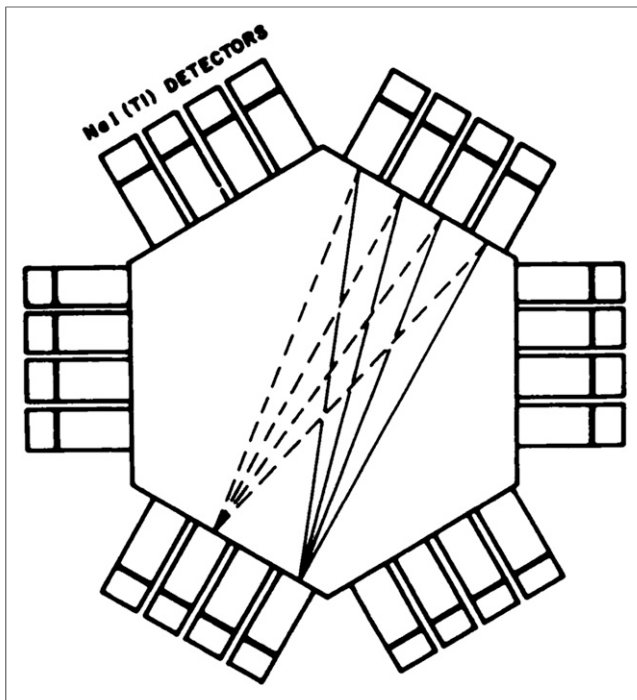
FIGURE 19. Schematic illustration of multiple coincidence logic possible with ACD of PETT.

or EDTA could be used for brain and kidney examinations; ^{68}Ga can be bound to transferrin because of its chemical similarity with indium and employed as a blood tracer; lung, liver, and spleen studies using particulate suspension could be performed with ^{68}Ga(OH)$_3$ particles or ^{68}Ga-labeled macroaggregated albumin. However, procedures and dosimetry will have to be studied before the practicality of these procedures can be evaluated. A number of positron-emitting radionuclides such as ^{11}C, ^{15}O, ^{13}N, and ^{18}F, currently employed in physiologic studies, offer the possibility of measuring metabolic activity. In general, the dedication of this system to positron emitting radionuclides may be less restrictive than the requirement of low photon energy imposed by the scintillation camera or those restrictions imposed by the chemical properties of technetium.

It is our opinion that transaxial reconstruction tomography provides a distinct improvement in nuclear medicine imaging and that there are a number of significant advantages in the use of annihilation coincidence detection.

REFERENCES

1. Hounsfield GN: Computerized transverse axial scanning (tomography). Part I: Description of system. Ambrose J: Part II: Clinical application. *Br J Radiol*. 1973;46:10l6–1047.
2. Kuhl DE, Edwards RQ: Image separation radioisotope scanning. *Radiology*. 1963;80:653–662.
3. Kuhl DE, Edwards RQ: Reorganizing data from transverse section scans using digital processing. *Radiology*. 1968;91:975–983.
4. Kuhl DE, Edwards RQ: The Mark III scanner. A compact device for multiple-view and section scanning of the brain. *Radiology*. 1970;96:563–570.
5. Kuhl DE, Edwards RQ, Ricci AR, et al: Quantitative section scanning using orthogonal tangent correction. *J Nucl Med*. 1973;14:196–200.
6. Todd-Pokropek AE: Tomography and the reconstruction of images from their projections. In *Proceedings of the Third International Conference on Data Handling and Image Processing in Scintigraphy*, Metz C, ed, Boston, June, 1973.
7. Todd-Pokropek AE: The formation and display of section scans. In *Proceedings of Symposium of American Congress of Radiology*, 1971, Amsterdam, Excerpta Medica, 1972, p 545.
8. Bowley AR, Taylor CG, Causer DA, et al: A radioisotope scanner for rectilinear, arc, transverse section and longitudinal section scanning. (ASS—The Aberdeen Section Scanner). *Br J Radiol*. 1973;46:262–271.
9. Myers MJ, Keyes WI, Mallard JR: An analysis of tomographic scanning systems. In *Medical Radioisotope Scintigraphy, vol*, vol 1, Vienna, IAEA, SM-164/48, 1972, pp 331–345.
10. Tanaka E: Multi-crystal section imaging device and its data processing. In *Proceedings of the Thirteenth Congress on Radiology*, Madrid, 1973, Amsterdam, Excerpta Medica, 1973, p 81.
11. Tanaka E, Shimizu T, Iinuma TA, et al: Digital simulation of section image reconstruction. *Natl Inst Radiol Sci (Japan)*, Report NIRS-12, 1973, pp 3–4.
12. Budinger TF, Gullberg GT: Three-dimensional reconstruction in Nuclear Medicine by iterative least-squares and Fourier transform techniques. *IEEE Med Sci* NS-. 1974;21 2–20.
13. Budinger TF, Gullberg GT: Three dimensional reconstruction of isotope distributions. *Phys Med Biol*. 1974;19:387–380.
14. Keyes JW, Simmon W: Computer techniques for radionuclide transverse section tomography and quantitative spatial (three dimensional) imaging. In *Sharing Computer Programs and Technology in Nuclear Medicine*, Clark FH, Maskewitz BF, Gurney J, eds, Oak Ridge, Tenn, USAEC Report CONF-730627, 1973, pp 190–201.
15. Oppenheim BE, Harper PV: Iterative three-dimensional reconstruction: A search for a better algorithm. *J Nucl Med*. 1974;15:520.
16. Wrenn FR, Good ML, Handler P: The use of positron-emitting radioisotopes for the localization of brain tumors. *Science*. 1951;113:525–527.
17. Brownell GL, Sweet WH: Localization of brain tumors with positron emitters. *Nucleonics*. 1953;11:No 11, 40–45.
18. Brownell GL, Burnham CA, Silensky S, et al: New developments in positron scintigraphy and the application of cyclotron-produced positron emitters. In *Medical Radioisotope Scintigraphy*, Vienna, IAEA, 1968, pp 163–176.
19. Burnham CA, Brownell GL: A multicrystal positron camera. *IEEE Med Sci* NS-. 1973;19 3, 201–205.
20. Chesler DA: Three-dimensional activity distribution from multiple positron scintigraphs. *J Nucl Med*. 1971;12:347–348.
21. Chesler DA: Positron tomography and three dimensional reconstruction techniques. In *Tomographic Imaging in Nuclear Medicine*, Freedman GS, ed. New York, Society of Nuclear Medicine, 1973, pp 176–183.
22. Dyson NA: The annihilation coincidence method of localizing positron-emitting isotopes and a comparison with parallel counting. *Phys Med Biol*. 1960;4: 376–390.
23. Mathews CME: Comparison of coincidence counting and focusing collimators with various isotopes in brain tumor detection. *Br J Radiol*. 1964;37: 531–543.
24. Cormack AM: Reconstruction of densities from their projections, with applications in radiological physics. *Phys Med Biol*. 1973;18:195–207.
25. Robertson JS, Marr RB, Rosenbaum M, et al: Thirty-two crystal positron transverse section detector. In *Tomographic Imaging in Nuclear Medicine*, Freedman GS, ed, New York, Society of Nuclear Medicine, 1973, pp 142–153.
26. Bracewell R, Riddle A: Inversion of fan-beam scans in radio astronomy. *Astrophys J*. 1967;150:427–434.
27. Ramachandran GN, Lakshminarayana AV: Three dimensional reconstruction from radiographs and electron micrographs: application of convolutions instead of Fourier transforms. *Proc Natl Acad Sci, USA*. 1971;68:2236–2240.
28. Smith P, Peters T, Bates R: Image reconstruction from finite numbers of projections. *J Phys A Math Nucl Gen*. 1973;6:361–382.

29. Cho ZH, Ahn A, Tsai C: Computer algorithms and detector electronics for the transmission x-ray tomography. *IEEE Trans Nucl Sci* NS-21, 1974;1:218, 1974.

30. Shepp LA, Logan BF: Some insights into the Fourier reconstruction of a head section. *IEEE Trans Nucl Sci,* NS-. 1974;21:21–43.

31. Gordon R, Bender R, Herman G: Algebraic reconstruction techniques (ART) for three-dimensional electron microscopy and x-ray photography. *J Theor Biol.* 1970;29:471–481.

32. Gilbert PFC: The reconstruction of a three-dimensional structure from projections and its application to electron microscopy. II. Direct methods. *Proc R Loud Soc [Biol].* 1972;182:89–102.

33. Marr RB: On the reconstruction of a function on a circular domain from a sampling of its line integrals. *J Math Anal Appl.* 1974;45:357–374.

34. Beck RN: Collimation of gamma rays. In *Fundamental Problems in Scanning,* Gottschalk A, Beck RN, eds, Springfield, 111, Charles C Thomas, 1968, pp 71–92.

35. Genna S, Farmelant MA, Burrows BA: Improved scintiscan resolution without sensitivity loss: "Constant resolution" collimator. In *Medical Radioisotope Scintigraphy, vol*, vol 1, Vienna, IAEA, 1969, pp 561–574.

36. Clarke LP, Laughlin JS, Mayer K: Quantitative organ-uptake measurement. *Radiology.* 1972;102:375–382.

37. Brownell GL: Theory of radioisotope scanning. *Int J Appl Radiat Isot.* 1958;3: 181–192.

38. Beck RN: A theoretical evaluation of brain scanning systems. *J Nucl Med.* 1961;2:314–324.

39. Hancock JC: *An Introduction to the Principles of Communication Theory.* New York, McGraw-Hill, 1951, p 18.

40. Welch MJ, Lifton JF, Ter-Pogossian MM: The preparation of millicurie quantities of oxygen-15 labeled water. *J Lab Cpds.* 1969;5:168.

41. Straatmann MG, Welch MJ: Enzymatic synthesis of nitrogen-13 labeled amino acids. *Radiat Res.* 1973;56:48–56.

42. Welch MJ, Ter-Pogossian MM: Preparation of short half-lived gases for medical studies. *Radiat Res.* 1968;36:580–587.

43. Harper PV, Lathrop KA, Krizek H, et al: Clinical feasibility of myocardial imaging with 13NH3. *J Nucl Med.* 1972;13:278–280.

44. Monahan WG, Tilbury RS, Laughlin JS: Uptake of ^{13}N-labeled ammonia. *J Nucl Med.* 1972;13:274–277.